Copper-promoted Nitrogen-doped Carbon Derived from Metal Organic Framework for Oxygen Reduction Reaction

Yunchao Xie[1], Chi Zhang[1], Xiaoqing He[2], Thomas Parker[4], Tommi White[2,3], Mark Griep[4], and Jian Lin[*1]

[1]*Department of Mechanical & Aerospace Engineering*, *University of Missouri*, *Columbia*, *Missouri 65211*, *United States*.

[2]*Electron Microscopy Core Facility, University of Missouri, Columbia, MO 65211, United States*

[3]*Department of Biochemistry, University of Missouri, Columbia, MO 65211, United States*

[4]*U.S. Army Research Laboratory, Weapons and Materials Research Laboratory, ATTN: RDRL-WM, Aberdeen Proving Ground, MD 21005-5069, United States*

Rational design of oxygen reduction reaction (ORR) electrocatalysts based on earth-abundant elements is imperative towards sustainable energy applications. Among various reported ORR electrocatalysts, transition metal (TM) ions-nitrogen atoms such as Fe-N_x and Co-N_x embedded in porous carbon matrix exhibit excellent catalytic activity. Nevertheless, comprehensive understanding of the electrocatalytic mechanism in these systems is still lacking, which demands extension of investigation to other TM-N/C systems such as the Cu-N/C system. However, they are quite under explored. Herein, we developed an ORR catalyst based on trace Cu promoted nitrogen-doped carbon (Cu-N/C) with Cu content as low as 0.13 at % *via* high temperature pyrolysis of Cu-adsorbed zeolite imidazole frameworks (Cu@ZIF-8) under Ar/H_2 atmosphere.

To perform these material characterizations, scanning electron microscopy (SEM) images using secondary electrons were firstly taken at 20 kV to investigate the topography of the samples. As shown in Figure 1B and Figure S2, both Cu-N/C-1 derived from ZIF-8/Cu ion precursor and N/C derived from pure ZIF-8 retained their initial dodecahedral morphology after high temperature pyrolysis. Elemental mapping images illustrate that carbon, nitrogen, and copper are uniformly distributed in Cu-N/C-1 (Figure 1C). Scan transmission electron microscopy-high angle annular dark field (STEM-HAADF) image of Cu-N/C-1 displays that formed Cu NPs with sizes of ~ 5 nm are supported on N/C (Figure 1D). More importantly, Cu-N/C-1 exhibits porous structures which enables more exposure of the active sites and fast mass/electron transfer during the ORR procedure. High-resolution TEM (HRTEM) image of one of the bright particles in STEM-HAADF image shows lattice fringe with a lattice spacing of 0.21 nm, which is attributed to the (111) plane of Cu NPs (Figure 1D).

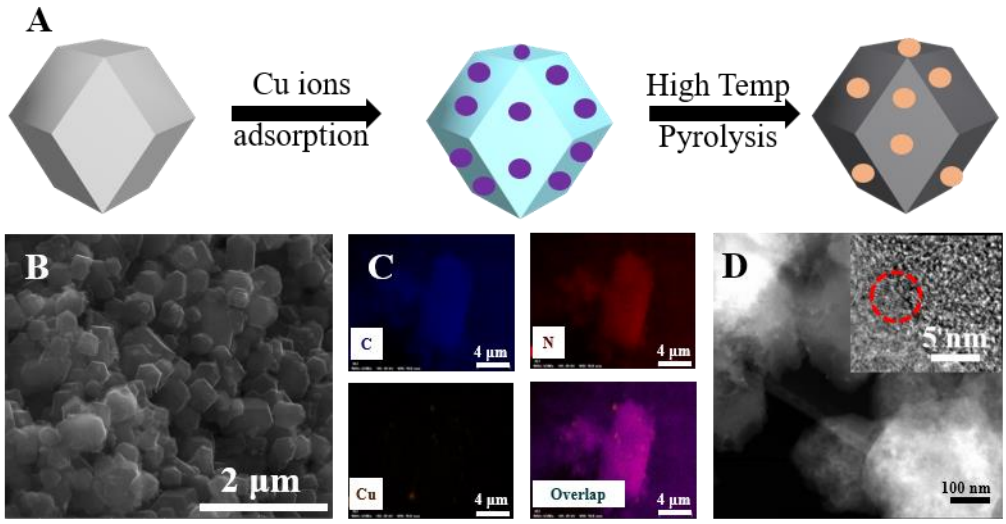

Figure 1. (A) Schematic of fabrication procedure for Cu-N/C catalysts. (B) SEM, (C) elemental mapping image, and (D) STEM-HAADF and HRTEM (inset) of Cu-N/C-1.

ORR activities of the electrocatalysts were first investigated by cyclic voltammetry (CV) measurements in O_2- or N_2-saturated 0.1 M KOH electrolytes. As shown in Figure 2A, Cu-N/C-1 exhibits a clear reduction peak in the O_2-saturated 0.1 M KOH electrolyte while in the N_2-saturated electrolyte no such a peak appears, suggesting the electrocatalytic activity of this hybrid catalyst toward ORR. The ORR activities of Cu-N/C-*x* electrocatalysts were further proved by the linear sweep voltammetry (LSV) curves at a scan rate of 10 mV/s in O_2-saturated electrolyte. As a comparison, N/C derived from pure ZIF-8 precursor and commercial Pt/C were also tested under the same conditions. Among the Cu-N/C-*x* electrocatalysts prepared with different micromole amount of copper ions in the precursors, the Cu-N/C-1 electrocatalyst exhibits the highest ORR activity. It shows a lowest onset potential of 1.029 V and half-wave potential ($E_{1/2}$) of 0.813 V, close to those of commercial Pt/C (1.001 V, and 0.821 V, respectively). The obtained diffusion-limited current density of 6.0 mA/cm^2 for Cu-N/C-1 is even larger than that of Pt/C (5.4 mA/cm^2) at 0.3 V (*vs*. RHE). Moreover, it is close to recent published Cu-N-C electrocatalsyts (e.g., Cu-N/C, CuNC/KB-400, CPG-900, 25% Cu-N/C, Cu/g-CN, and Cu_3N100@CNT) and also comparable to very popular Fe-N_x/C or Co-N_x/C. Under the same measurement conditions, N/C shows the poorest activity with $E_{1/2}$ of 0.775 V, suggesting that the introduction of Cu species makes contribution to the ORR and that the N-Cu(II)-Cu^0 sites could serve as the active sites for catalyzing the ORR. Cu-N/C with the lower (Cu-N/C-0.5) or higher (Cu-N/C-12) copper concentration showed poorer ORR performance compared to those of Cu-N/C-1 and Pt/C. A lower amount of Cu (Cu-N/C-0.5) will result in insufficient Cu(II)-N sites and Cu^0 NPs, while an excessive amount of Cu (Cu-N/C-12) will form more metallic Cu NPs. Furthermore, the Tafel slopes of N/C, Cu-N/C-1 and Pt/C were calculated based on the corresponding LSV curves at lower potentials where the ORR rate depends on the surface reaction rate (Figure 3C). Cu-N/C-1 exhibits a much smaller Tafel slope (57.5 mV/dec) in comparison with those of Pt/C (81.9 mV/dec) and N/C (82.9 mV/dec), demonstrating that the moderating doping of Cu species in N-doped

carbon can greatly enhance ORR kinetic process.

It is known that the ORR can follow a $2e^-$ pathway with HO_2^- as an intermediate or a $4e^-$ pathway as OH^- as the final product. From an energy conversion perspective, the latter one is preferred. In the $4e^-$ pathway, it has been suggested to go through two-oxygen atom side and/or bridge adsorption for oxygen dissociation simultaneously. The electron transfer number per oxygen molecule (n) and peroxide yield (HO_2^- %) can demonstrate the electron transfer kinetics and pathway. As shown in Figure 3D, the measured n increases and the HO_2^- yield is suppresses in the Cu-N/C-1 catalyst in comparison to those of N/C, indicating the importance of trace Cu in the hybrid catalyts. To gain further insights into the reaction kinetics and pathways, the LSV curves of Cu-N/C-1 at different rotating speeds, and the corresponding Koutechy-Levich (K-L) plots are shown in Figure 2E and 2F, respectively. As the rotation speed increases, the onset potentials for the Cu-N/C-1 remain constant (Figure 2E), while the current density is increased owing to the increased mass transport at a higher rotating speed. The K-L plots (Figure 2F) of Cu-N/C-1.0 under various potentials exhibit excellent linearity and near coincidence, which indicates first-order reaction kinetics and consistent electron transfer number (n) value per oxygen molecule. For Cu-N/C-1, the n value is calculated to be ~3.8, in good agreement with an efficient $4e^-$ transfer pathway.

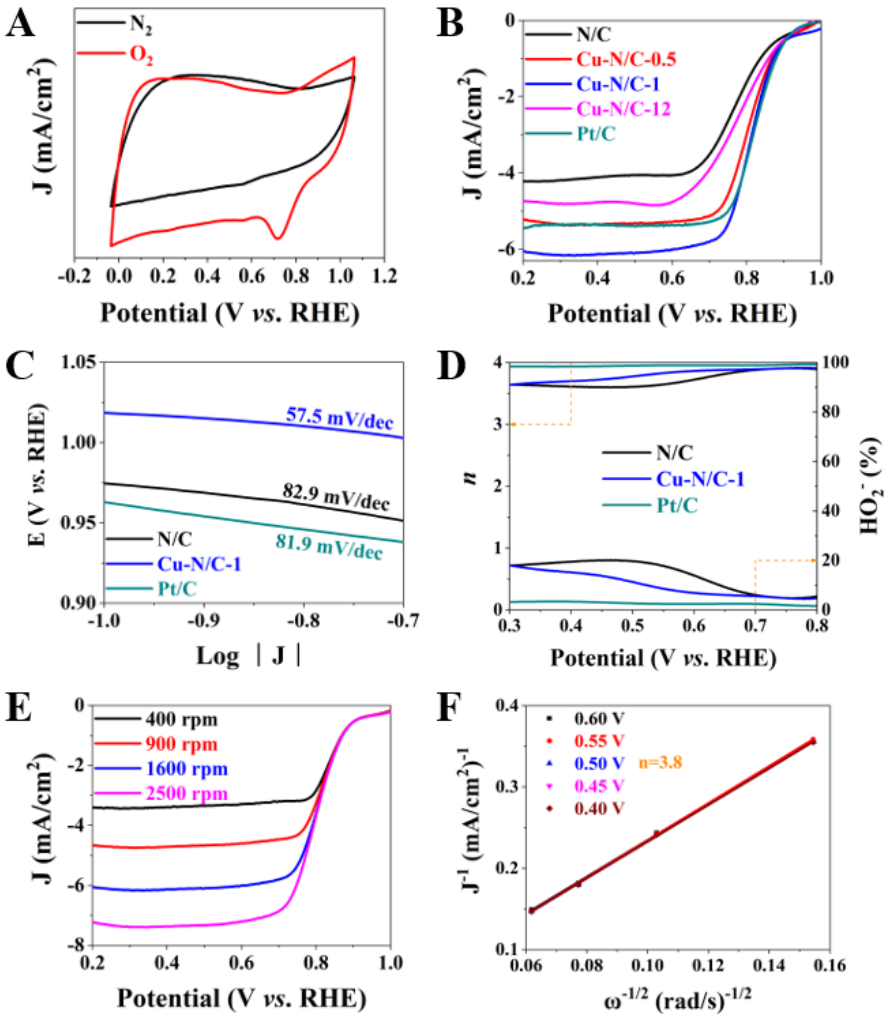

Figure 2. (A) Cyclic voltammetry (CV) curves of Cu-N/C-1 in O_2 or N_2-saturated 0.1 M KOH electrolyte at a scan rate of 100 mV/s. (B) Linear sweep voltammetry (LSV) curves of Cu-N/C-*x*, N/C and Pt/C in O_2-saturated 0.1 M KOH electrolyte at a scan rate of 10 mV/s and rotating speed of 1600 rpm. (C) Tafel slope, (D) electron transfer number (*n*) and HO_2^- yield of Cu-N/C-1, N/C and Pt/C at a potential range from 0.3 V to 0.8 V (*vs*. RHE). (E) LSV curves, and (F) corresponding K-L plots of Cu-N/C-1 at different rotating speeds (400 ~ 2500 rpm) in O_2-saturated 0.1 M KOH electrolyte at a scan rate of 10 mV/s.